Single crystalline LuAG fibers for homogeneous dual-readout calorimeters

2013 JINST 8 P09019

(http://iopscience.iop.org/1748-0221/8/09/P09019)

PUBLISHED BY IOP PUBLISHING FOR SISSA MEDIALAB

RECEIVED: *June 4, 2013*
ACCEPTED: *August 26, 2013*
PUBLISHED: *September 26, 2013*

Single crystalline LuAG fibers for homogeneous dual-readout calorimeters

K. Pauwels,[a,b,1] **C. Dujardin,**[b] **S. Gundacker,**[a] **K. Lebbou,**[b] **P. Lecoq,**[a] **M. Lucchini,**[a,c] **F. Moretti,**[b] **A.G. Petrosyan,**[d] **X. Xu**[b] **and E. Auffray**[a]

[a] *European Organization for Nuclear Research, CERN, CH-1211 Geneva, Switzerland*
[b] *Institut Lumière Matière, UMR5306 Université Lyon 1-CNRS, Villeurbanne cedex, France*
[c] *University of Milano-Bicocca, Piazza dell'Ateneo Nuovo 1, Milano, 20125, Italy*
[d] *Institute for Physical Research, NAS of Armenia, Ashtarak-2, 0203, Armenia*

E-mail: pauwels@cern.ch

ABSTRACT: For the next generation of calorimeters, designed to improve the energy resolution of hadrons and jets measurements, there is a need for highly granular detectors requiring peculiar geometries. Heavy inorganic scintillators allow compact homogeneous calorimeter designs with excellent energy resolution and dual-readout abilities. These scintillators are however not usually suited for geometries with a high aspect ratio because of the important losses observed during the light propagation. Elongated single crystals (fibers) of Lutetium Aluminium garnet (LuAG, $Lu_3Al_5O_{12}$) were successfully grown with the micropulling-down technique. We present here the results obtained with the recent fiber production and we discuss how the light propagation could be enhanced to reach attenuation lengths in the fibers better than 0.5 m.

KEYWORDS: Calorimeters; Calorimeter methods; Particle identification methods; Cherenkov detectors

[1] Corresponding author.

doi:10.1088/1748-0221/8/09/P09019

Contents

2013 JINST 8 P09019

1 Introduction

High Energy Physics experiments at future colliders (e.g. HL-LHC, ILC, CLIC) will have to face challenging operating conditions with unprecedented luminosities and collision rates. The next generation of detectors will require, in addition to excellent timing properties, a significantly better jet resolution, especially in the forward region. At present, the R&D effort is mainly oriented towards two concepts: the particle flow approach [1, 2] and the dual readout scheme [3, 4]. Within the former, both the electromagnetic and the hadronic calorimeters are very finely segmented in order to allow very efficient pattern recognition and thus identify and track all particles in a jet. The number of channels of such detectors sets however complex engineering problems. In dual-readout designs, the energy resolution is improved by measuring, on an event by event basis, the electromagnetic fraction of hadronic showers. This can be achieved by detecting both the ionization and the Cherenkov signals. To efficiently dissociate the two types of signals, such calorimeters also require a relatively high granularity of the detector. Geometries with a high aspect ratio do not usually favor heavy inorganic scintillators because of the important losses observed during the light propagation. As a result, dual-readout designs are often based on sampling calorimeters which do not benefit from the excellent energy resolution of homogeneous systems. Nevertheless, as opposed to particle flow detectors, dual-readout calorimeters only require a limited number of channels: all ionization and Cherenkov signals can be summed optically or electronically.

1.1 Calorimetry with meta-crystals

To circumvent the limitations of these two concepts, we proposed earlier a third approach based on meta-crystals [5, 6]. In this concept, trunks of *cables* constructed from heavy inorganic single crystalline fibers are assembled to form the detector blocks. This solution provides the appropriate segmentation, is dense enough to avoid the necessity of an absorber (thereby excluding sampling fluctuations) and presents dual-readout capabilities. Extrinsic scintillators consist of materials doped with luminescent ions. When undoped, they often do not emit light under ionizing radiation (or at least, the scintillation yield is significantly lower at room temperature and exhibit a different time response). Both doped and undoped materials can thus be assembled to measure respectively the scintillation and Cherenkov signals. The system is then capable of disentangling the electromagnetic (em) and non-em components of a shower with a uniform Moliere radius R_M, radiation and interaction lengths X_0 and λ_I.

1.2 Lutetium Aluminium garnet as candidate material

Lutetium Aluminium garnet (LuAG, $Lu_3Al_5O_{12}$) is considered as an attractive scintillating material and its properties have been extensively studied over the past ten years. A review of the research and development can be found in [7]. The use of LuAG for production of meta-crystals was proposed earlier [6, 8]. Some of its relevant properties are summarized in table 1. Because of its high density of 6.73 g/cm^3 and relatively short radiation and interaction lengths of respectively 1.41 cm and 23.3 cm, LuAG is a relevant candidate as host material. When undoped, it is an efficient Cherenkov radiator because of its high refractive index (2.14 at 190 nm and 1.85 at 520 nm) [9, 10] and thus its low Cherenkov threshold (97 keV for electrons). Fast scintillation processes can in addition be activated by doping the host matrix with some specific rare-earth ions. Among the lanthanide series, Praseodymium and Cerium show very good performances. Pr^{3+}- and Ce^{3+}- based scintillation yields respectively 16 000 and 25 000 photons per deposited MeV [11, 12] and relatively short decay time due to parity allowed electric dipole d-f transitions (respectively 25 and 60 ns) [13, 14]. The parasitic slow component observed in addition under ionizing radiation excitation can efficiently be suppressed with Gallium co-doping as reported in [15]. The two dopants also differ by their emission spectrum: the Ce^{3+} emission peaks at 520 nm whereas the Pr^{3+} emission spectrum lies partly in the UV with two emission bands peaking at 320 and 370 nm. The choice of the photodetector to be used to measure the scintillation light will then play a role in the dopant selection. Cerium ions may as well be favored if Cherenkov and scintillation signals need to be separated (e.g. for dual-readout purposes).

1.3 Micropulling-down technology

Heavy inorganic scintillators are traditionally grown by Czochralski and Bridgman methods which usually yield large ingots. Obtaining fiber-shaped samples then involves non-negligible machining processes (i.e. cutting and polishing). Shaped crystal growth is another possible approach: the micropulling-down technology (μPD) allows the growth of single crystals directly shaped into fibers. Because of its high pulling rate and its ability to grow multiple samples simultaneously, μPD also displays a good adaptability for large-scale production. The process is based on a crucible designed with a micro-nozzle die (of diameter ranging from 300 μm to 3 mm) which constrains the

2013 JINST 8 P09019

Table 1. Physical and optical properties of LuAG crystals. Values labeled with * and $^\bullet$ are for crystals doped with Praseodymium and Cerium respectively.

Physical properties		Optical properties	
Density	6.73 gr/cm^3	Light yield	16000* - 25000$^\bullet$ ph/MeV
Zeff	62.9	Emission wavelength	320,370* - 520$^\bullet$ nm
Radiation length X_0	1.41 cm	Decay time	25* - 60$^\bullet$ ns
Interaction length λ_I	23.3 cm	Refractive index	1.85 at 520 nm
Melting point	2060 °C	Cherenkov threshold	97 keV
Thermal expansion	8.8 10^{-6}/°C	Max Cherenkov angle	57°
Thermal conductivity	31 W/m°C	Total reflection angle	33°

melt flow before the contact with the seed crystal. Rod-like single crystals of the desired orientation can then be grown. Because of its mechanical and chemical properties, LuAG is favored in this shaped crystal growth with respect to other inorganic scintillators (e.g. Lutetium oxyorthosilicate, LSO). Although square and hexagonal fibers can be produced with μPD, a round section for the LuAG fibers was selected here to favor optical quality of the samples and shape reproducibility.

1.4 Specificities of the fiber geometry

Up to 30 000 ph/MeV can be extracted from LuAG crystals of high quality [11, 12] but such values are unlikely to be achieved with a fiber shaped scintillator. It was shown in [16] that heavy inorganic scintillating crystals of high aspect ratio do not yield efficient extraction of the generated light. And this is especially valid when surface defects are observed on the samples. The work presented here therefore focused on two distinct aspects of the detection of the scintillation light: the light production and the light propagation. While the former depend on the crystal quality, the second is governed by the geometry of the sample and the surface state. The early batches of fibers produced displayed light attenuation lengths equal or worse than 5 cm [11]. The quality of the light propagation was thus identified as the key parameter to optimize in order to ensure the possibility to assemble a calorimeter of relevant size ($L \gtrsim 1.2\ \lambda_I$). An extensive screening campaign of the growth parameters has therefore been performed. Only scintillating fibers (LuAG:Ce) were investigated at first since it was shown that doping LuAG with rare-earth ions of large ionic radius (i.e. Ce^{3+}) can cause non-negligible surface defects [17, 18]. The undoped fibers are therefore considered to be grown with equal or better optical quality.

2 Experimental procedures

2.1 LuAG fibers and LuAG crystals

Single crystalline fibers (2 mm diameter) of LuAG:Ce have been grown at ILM by the μPD technique along the $\langle 111 \rangle$ crystallographic axis. The growth process was initiated once a direct contact has been established between the oriented seed crystal and the capillary die at the bottom of the iridium crucible. For a given geometry of crucible, the critical tuning parameters are the pulling rate, the applied heating power and the quality of the raw materials. The exact technical details

2013 JINST 8 P09019

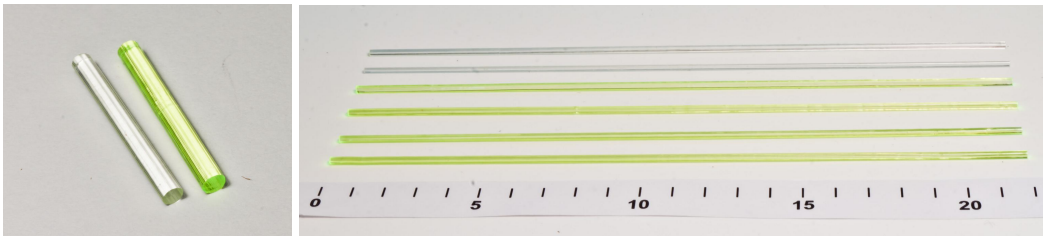

Figure 1. Pictures of LuAG single crystalline fibers with a diameter of 2 mm and lengths of 2 and 22 cm (left and right respectively).

are being published in a different communication [19]. A list of the samples is provided in table 2. Some pictures of a set of LuAG fibers are also displayed in figure 1.

For comparison, bulk single crystals of LuAG:Ce were grown at IPR by the vertical Bridgman technique [20] using high purity (99.99%) oxides and molybdenum containers under an enclosed Ar/H_2 (90/10 vol %) atmosphere. The starting melt concentration of Ce was around 1.0 at.% and the crystals were grown along the $\langle 100 \rangle$ crystallographic axis. Crystals of dimensions $2\times2\times8\,mm^3$ and $2\times2\times45\,mm^3$ polished on all sides were cut from the as-grown ingots.

2.2 Light output and attenuation measurements

In high energy physics, scintillating crystals are not usually required to have a high light yield. On the other hand, low values of light yield significantly affects the characterization studies because the energies of the γ-photons generated by usual radioactive sources involved in standard scintillator characterization (0.2-2 MeV) only give rise to a very low number of photons. Drastic constrains are thus set on the selection of an efficient and reliable readout scheme. We selected multi-pixels photon counters (S10931-050P MPPC from Hamamatsu). This choice was motivated by their higher quantum efficiency (around 22%) in the 520-600 nm region (corresponding to the Ce^{3+} emission spectra in LuAG). Besides, these detectors show excellent photon counting probabilities at low light levels. A dedicated instrumental amplifier (gain of 180) was designed because of the rather small amplitude of the measured signals. It was connected directly to the MPPC output with very short connector pins. The amplifier was operated in a differential mode in order to cancel common-mode noise and pick-up that would otherwise become predominant and significantly alter the measurements of very low number of photoelectrons. In such operating conditions, the single photoelectron response was estimated to be around 30 pC (see figure 3-*a*).

Light output measurements were performed with two MPPCs coupled with optical grease (Rhodorsil Paste 7) of refractive index $n = 1.41$ to the ends of the fiber (see figure 2). This double readout (front and back) was chosen in order to increase the number of photons collected and also to be able to measure the attenuation of the light within the fiber. Each γ-ray interaction shares the scintillation light into the forward and the backward direction. The comparison of these two signals then allows estimating the light losses occurring during the light propagation along the fiber axis. The interaction region was selected with an electronic collimation based on two back-to-back 511 keV γ-rays resulting from the positron annihilation of a Na^{22} radioactive source. One of the γ-rays was detected with a $2\times2\times5\,mm^3$ LYSO crystal coupled to a third MPPC. This fast and bright signal was used to initiate a trigger condition. If subsequently an event was detected in either of

2013 JINST 8 P09019

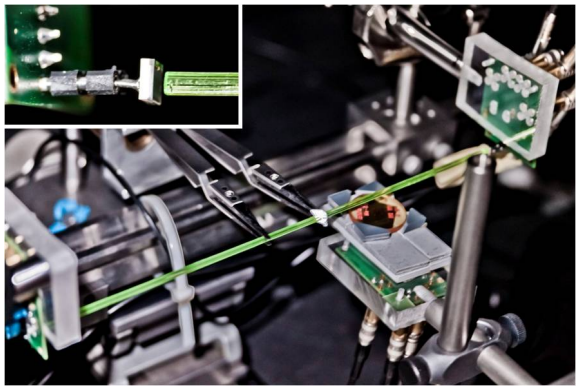

Figure 2. Pictures of the experimental setup used to measure the light output and the light attenuation of the LuAG crystals and fibers.

the MPPCs coupled to the fiber, within a time window of 400 ns (corresponding to the integration time), the trigger was confirmed. The threshold level for this second trigger was set just below the single photoelectron level.

It is noteworthy that, when only a few tens of photoelectrons are collected from the MPPCs, a non-negligible jitter is observed on the detection of the first photoelectron. An integration window started on this event led to fluctuations in the integration time. This in turn resulted in additional fluctuations in the measured pulse area when the selected integration time was set too short to integrate the entire scintillation pulse. On the other hand, larger integration times led to a predominant pedestal peak due to the relatively high dark count rate of MPPCs ($\sim$1.5 MHz at 20°C). We thus decided to use the signal of the LYSO tagging crystal as timestamp and to integrate the front and back signals collected from the LuAG fibers on a time window opened 50 ns before the tagging time. The time window was opened for 450 ns, which is a good compromise between number of photoelectrons collected and influence of the dark count rate.

The trigger conditions described here above combine a very low threshold, a relatively low amount of noise triggers and a well-defined time window for the integration of the scintillation pulses. They were achieved experimentally with a digital oscilloscope (LeCroy WaveRunner 104XI, bandwidth of 1 Ghz). We would like to mention here some limitations in the use of MPPCs for light output measurements. Non-linear effects can be observed at high photon rates due to the limited number of single photon avalanche diodes (SPADs). The number of these microcells and their dead time will determine the exact threshold in number of photons from where the detection will be underestimated. For values below 300 phe, as discussed in this paper, we expect the deviation to be negligible ($<$4% for the brightest samples). On the other hand, cross-talk and after-pulsing tend to overestimate the number of photoelectrons detected (one photon may yield more than one SPAD firing). Light output measurements therefore have to be considered carefully. The estimations discussed here do not aim at providing an absolute number of photons generated but rather aims at providing a relevant figure of merit for the light output. This figure of merit is particularly meaningful since MPPCs are an excellent choice of photodetector for high energy experiments because of their robustness, their low cost and their insensitivity to magnetic fields.

2013 JINST 8 P09019

3 Light output of LuAG fibers

For the light output measurements, the γ-rays interaction region was restricted to the middle of the LuAG fiber (through the electronic collimation described earlier). Examples of charge spectra obtained from the sum of the front and back readouts are provided in figure 3. Around 100 photoelectrons could be collected for a LuAG fiber of 2 cm (see red curve in 3-*b*). The 22 cm long fibers displayed charge spectra with a photopeak almost not distinguishable (see black curve in 3-*b*). The estimated components of the pedestal, the back scattered peaks, the Compton continuum and the photopeak are shown in 3-*c*. They were computed by a simultaneous fit based on formula 3.1:

$$y(x) = \underbrace{A_{\text{ped}}\, e^{-\frac{x^2}{2\sigma_{\text{ped}}^2}}}_{\text{pedestal}} + \underbrace{A_{\text{bsc}}\, e^{-\frac{(x-X_{\text{bsc}})^2}{2\sigma_{\text{bsc}}^2}}}_{\text{back scattered}} + \underbrace{\frac{A_{\text{cpt}}}{\sqrt{1+\left(\frac{511}{340.7}\frac{x}{X_0}\right)^{w_{\text{cpt}}}}}}_{\text{Compton continuum}} + \underbrace{A_0\, e^{-\frac{(x-X_0)^2}{2\sigma_0^2}}}_{\text{photopeak}} \tag{3.1}$$

Due to the low number of photoelectrons, the four components do not separate easily as opposed to traditional charge spectra obtained with crystals with a higher light output. For the 22 cm long LuAG fiber, we estimate the light output to be around 60 phe per 511 keV γ-ray. We also measured, in the same experimental conditions, a $2\times2\times45$ mm^3 LuAG crystal cut out of a Bridgman-grown ingot and mechanically polished. This crystal, displaying a very good transparency, yielded around 360 phe per 511 keV γ-ray.

The light outputs measured here are much lower as opposed to the 16 000 ph/MeV traditionally measured on LuAG:Ce crystals with similar integration times [12]. The experimental conditions differ however significantly and many factors have to be taken into consideration before trying to compare the light yield of the different types of crystals. In section 5, we will summarize the different contributions involved. In the case of crystals shaped into elongated geometries, the propagation of the scintillation light becomes a dominant parameter. Therefore we will first discuss in more detail how to measure it experimentally and what are the ways to improve it.

4 Light propagation in LuAG fibers

4.1 Attenuation profiles

Computing the attenuation profiles of the scintillation light using a Na^{22} radioactive source is usually achieved by recording the light output of the total absorption events, for a range of positions of the radioactive source. As described in section 3, the charge spectra acquired with the LuAG fibers did not present features which could be clearly identified. We therefore decided to select events yielding a number of photoelectrons greater than the estimated position of the photopeak. This selection was more restrictive than usual but ensured that a great part of the Compton events was rejected. Since this threshold was estimated with a rather poor accuracy, the measurements could be biased by an event selection scheme which was not necessarily identical for all the γ-ray interactions. Usually the sum of the front and back signals is considered in order to minimize possible changes in this events selection. This sum of signals is yet only significantly independent of the position z if the attenuation length is in the order of the sample length. For illustration, the

2013 JINST 8 P09019

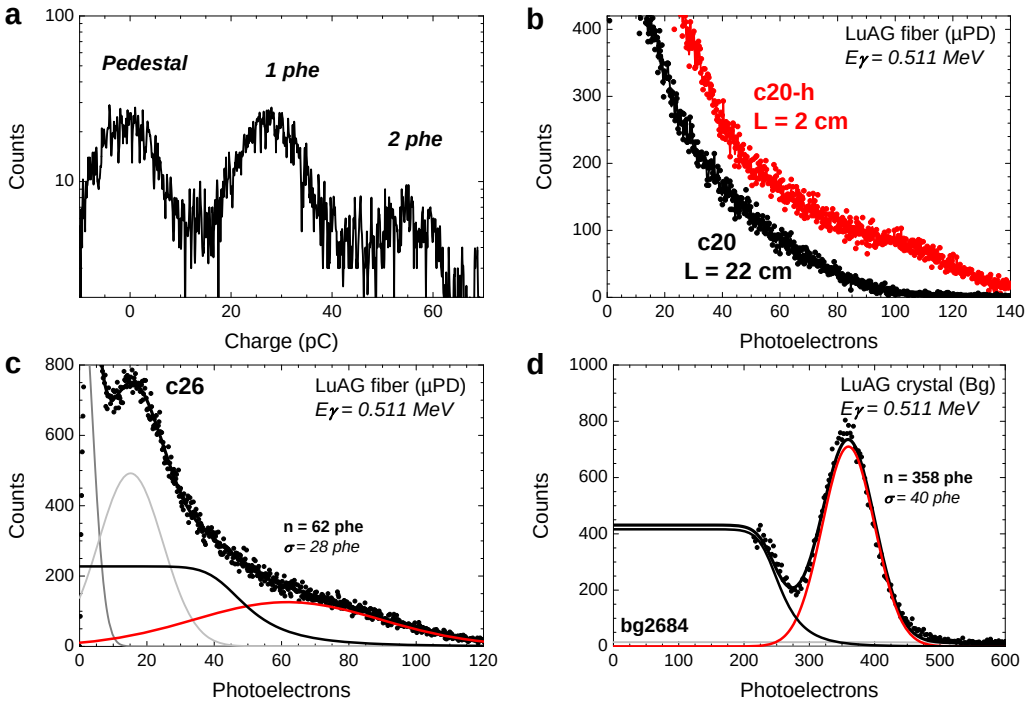

Figure 3. (a) Spontaneous firing of the MPPC single photon avalanche diodes (SPADs). (b) Charge spectrum measured with a Cerium-doped LuAG fiber (c20) cut to 2 cm (red curve) and 22 cm (black curve). (c) Emphasize of the photopeak, the Compton continuum, the backscattered peaks and the pedestal for fiber c26. (d) Charge spectra measured with a Bridgman-grown crystal.

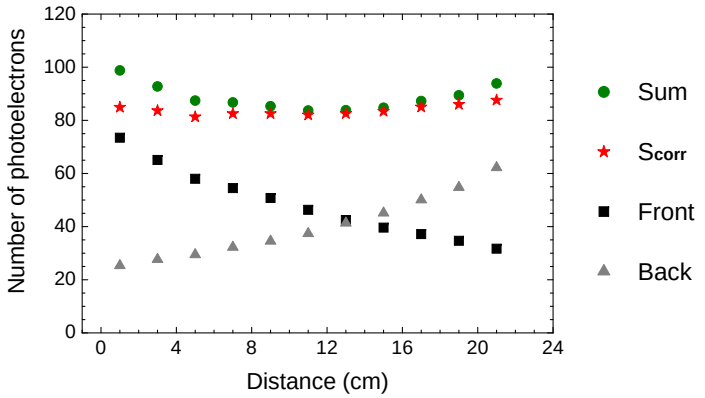

Figure 4. Number of photoelectrons collected by the front and back photodetectors as a function of the radioactive source position. The sum and the weighted sum S_{corr} are also displayed.

front, back and sum signals acquired with the LuAG fiber *c*22 are plotted in figure 4 for different positions of the Na^{22} source. These signals were calibrated and are expressed in photoelectrons.

We noted that, if the positions of the interactions could be estimated, it would be possible to define a variable which would stay constant in a wider range. This information is actually accessible from the ratio of the front and back signals since this ratio is linked to the position *z* of

2013 JINST 8 P09019

the radioactive source and the light attenuation length in the crystal λ_{att} by:

$$\frac{S_{\text{Back}}(z)}{S_{\text{Front}}(z)} = \exp\left(2\,\frac{z}{\lambda_{att}}\right) \tag{4.1}$$

A natural choice of variable, theoretically independent of the γ-ray interaction point z, can then be defined as:

$$S_{\text{corr}} = S_{\text{Front}}(z)\ \exp\left(\frac{z}{\lambda_{att}}\right) + S_{\text{Back}}(z)\ \exp\left(-\frac{z}{\lambda_{att}}\right) \tag{4.2}$$

which is easily re-written into:

$$S_{\text{corr}} = 2\,S_{\text{Front}}(z)\sqrt{\frac{S_{\text{Back}}(z)}{S_{\text{Front}}(z)}} \tag{4.3}$$

As predicted, we can see from figure 4 that, for fiber $c22$, the weighted sum S_{corr} provides a flatter profile as compared to the sum signal. As a result, the event selection was thus performed for all samples based on this method. To further improve the reliability of the attenuation curves, we also decided to combine both front and back signals for the computation of the attenuation length. To achieve this, we define a dimensionless variable M_{FB} characterizing the light sharing between the front and the back readouts as:

$$M_{FB}(z) = \sqrt{\frac{S_{\text{Front}}(z)}{S_{\text{Back}}(z)}} \tag{4.4}$$

We note that $ln(M_{FB})$ scales linearly with the attenuation length. Plotting $ln(M_{FB})$ as a function of the source position then allows to compute the attenuation length, as illustrated for fiber $c22$ in figure 5. This method was applied to a set of LuAG fibers grown by μPD and also to a commercial scintillating plastic fiber (bc20 from St. Gobain) and a LuAG crystal grown by the Bridgman technique. The last two samples served as reference. The obtained attenuation curves are plotted in figure 6 and the attenuation lengths computed are summarized in table 2. The error bars provided on the plots represent the statistical error in the computation of the relative position M_{FB}.

As opposed to the early batches of fibers [11], we observe here a significant improvement of the light propagation in the LuAG fibers grown recently. Systematic scans of the growth parameters allowed identifying optimized conditions which led to a better surface state. The best samples were grown with a pulling rate around 0.25-0.35 mm/min. We notice however non-negligible differences in the surface quality of the samples, although grown with very similar parameters. A fine tuning of the conditions during the growth is necessary to reach light attenuation lengths better than 24 cm (samples $c22$ and $c31$).

We measured an attenuation length of around 14 cm for a Bridgman-grown crystal (see right plot of figure 6), which is comparable to the value of 17 cm recently measured on a Czochralski-grown crystal [21]. We can therefore conclude that, with these readout conditions, the LuAG fibers grown by μPD, although yielding a rather low light output (as described in section 3), present a better homogeneity of the light response, as compared to crystals grown by conventional growth methods. The quality of the light propagation is actually very similar to the one obtained with plastic scintillators (see right plot of figure 6), often considered as a reference in this respect.

2013 JINST 8 P09019

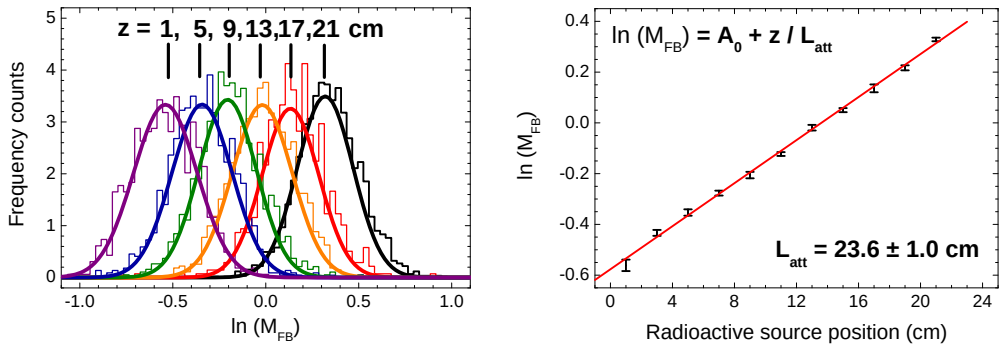

Figure 5. Illustration (for fiber c22) of the method used to characterize the light attenuation in the different LuAG samples. For each position of the Na^{22} source, the average $ln(M_{FB})$ is determined through a Gaussian fit (left). A linear fit subsequently provides the attenuation length (right).

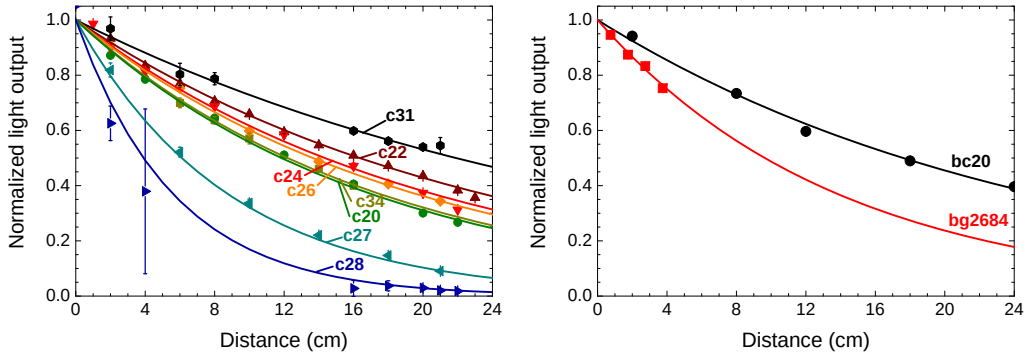

Figure 6. Attenuation profiles of the scintillation light generated by 511 keV γ-photons measured on a set of LuAG fibers (left), a plastic scintillator and Bridgman-grown LuAG crystal (right). Silicon grease of index 1.41 was used as coupling media between the samples and the photodetectors.

Given their excellent optical quality, it is rather surprising that LuAG crystals grown by conventional methods present a lower attenuation length as compared to some of the fibers grown by μPD. It was nevertheless demonstrated earlier that the crystal edges cause a non-negligible amount of light diffusion and absorption [16]. As a result, the numerous reflections do not occur without losses and the attenuation length quickly degrades for large collection angles. For short crystals (more accurately for crystals with a moderate aspect ratio), this effect is minimal but when high aspect ratios are considered, this effect becomes predominant.

It is also important to point out the primordial role of the exact nature of the light being collected. The reason why the LuAG fibers have a better homogeneity in the light response is mainly due to the fact that the fraction of the light which reaches the photodetector propagates in the fiber with a small angle. By contrast, the crystals cut from large ingots and polished allow the propagation of the light on a much wider set of angles. This results in a better light collection (higher light output) but a rather poor homogeneity of the response since the photons can follow a variety of different paths. Furthermore, photons emitted at large angles, which are more numerous (by solid angle considerations) are more likely to experience multiple bouncing and therefore more likely to be absorbed before reaching the photodetector.

2013 JINST 8 P09019

Table 2. Attenuation lengths measured on a set of LuAG fibers grown by μPD, a plastic scintillator and a LuAG crystal grown by the Bridgman technique. For the samples grown by μPD, some relevant growth parameters are provided for comparison.

Fibers grown by micro-pulling down				
Fiber	Pulling rate	Ce doping	Raw material	λ_{att}
C20	0.25 mm/min	0.1 at.%	Cz crystals	17.1 ± 1.2 cm
C22	0.25 mm/min	0.1 at.%	Cz crystals	23.6 ± 1.0 cm
C24	0.25 mm/min	0.1 at.%	Cz crystals	20.7 ± 1.3 cm
C26	0.25 mm/min	0.1 at.%	Cz crystals	19.7 ± 0.7 cm
C27	0.30 mm/min	0.1 at.%	Cz crystals	8.8 ± 0.6 cm
C28	0.30 mm/min	0.1 at.%	Cz crystals	5.6 ± 0.2 cm
C31	0.30 mm/min	0.1 at.%	μPD fiber	31.6 ± 3.7 cm
C34	0.32 mm/min	0.1 at.%	Cz crystals	17.6 ± 1.5 cm

Reference samples		
bg2684	Crystal grown by the Bridgman technique	13.9 ± 2.2 cm
bc20	Commercial plastic scintillating fiber	25.4 ± 2.3 cm

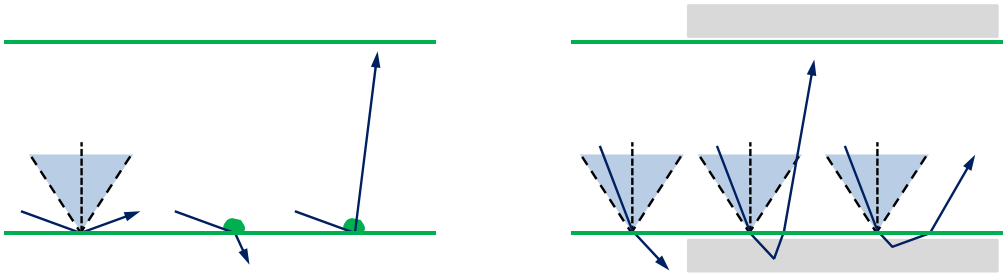

Figure 7. Sketch illustrating the different scenarios for a photon traveling in a LuAG fiber in the absence of wrapping (left) and when the fiber wrapped with a reflecting material (right).

As illustrated in the left sketch of figure 7, some of the photons propagating by total internal reflections can encounter a surface defect which will scatter this light. The photons can then either escape the crystal or be redirected with a larger angle which will increase the probability to have further interactions with surface defects. The concentration of defects on the surface of the LuAG fibers studied here reached a value which is a good compromise between the amount of light collected and the quality of the propagation.

4.2 Influence of the fiber environment

The amount of light collected with the LuAG fibers grown by μPD being relatively low, it could be worth to try to increase the light output by collecting the photons which exited the crystal through the lateral surface. As discussed in the previous section, this has to be done with care so that the gain in light is not counterbalanced by a loss in the light propagation. This is not straightforward since most usual wrappings and coatings have a refractive index significantly lower than LuAG.

2013 JINST 8 P09019

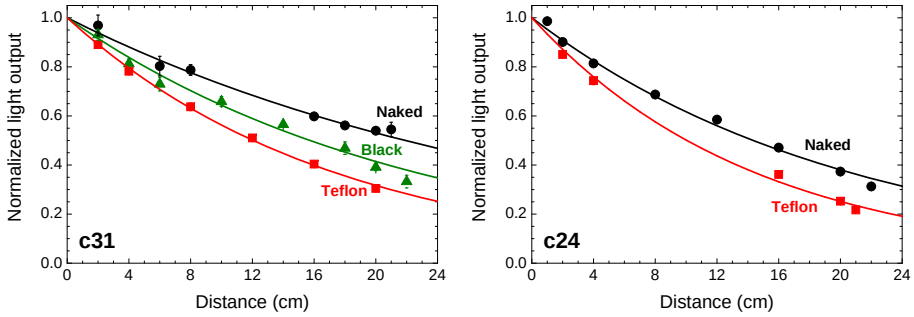

Figure 8. Attenuation profiles of the scintillation light generated by 511 keV γ-photons measured on two LuAG fibers. The samples were measured naked, with Teflon wrapping and black paint. Silicon grease of index 1.41 was used as coupling media between the samples and the photodetectors.

As illustrated in the right sketch of figure 7, the photons are therefore re-injected in the scintillator with a rather large angle, which is not favorable from the point of view of light propagation.

We investigated here only two cases: a Teflon wrapping which is a diffusive reflector commonly used for light output improvement and a coating with black paint. We decided to add the latter case to the study because it will probably be necessary to absorb the escaping photons to avoid cross-talk with neighboring fibers. The corresponding attenuation curves are provided for the LuAG fibers $c24$ and $c31$ in figure 8. As suspected, no improvement of the light attenuation was observed, the fibers wrapped with Teflon had their attenuation lengths decreased from $\sim$32 cm (resp. $\sim$21 cm) to $\sim$18 cm (resp. $\sim$15 cm). The fiber which was painted in black led to a light output reduced by around 48% but the light attenuation was not significantly altered. These two facts confirm the important role of the surface defects in the low light output and the good attenuation properties measured on the LuAG fibers.

4.3 Selection of the light collected

One possible way to minimize light attenuation in LuAG fibers is to avoid interactions with their surface. From this point of view, artificially reducing the collection angle to only consider light traveling straight (or within a certain collection cone) to the fiber ends is an interesting approach. We suspected that the LuAG crystals showed moderate attenuation properties because of the wide angle of collection of the photons. To confirm this, we measured the attenuation profiles with a 2 mm air gap between the fibers ends and the photodetectors. The presence of this air gap enabled us to select a narrower collection angle. As illustrated in figure 9, this limits the number of bouncing of the scintillation photons collected.

The results obtained with the 2 mm air gap are compared to the one obtained with optical grease in figure 10 for a LuAG fiber, a LuAG crystal and a plastic scintillator. For the crystal cut out of a Bridgman-grown ingot and polished, the light response became independent of the excitation point in presence of an air gap. The measured attenuation length could not be estimated since the measurement was not sensitive enough with a 4.5 cm long crystal. The value is however very likely to be in the order of a few meters. Such values are compatible with the excellent optical quality of the LuAG crystal. The fact that, for the same crystal, both moderate and excellent attenuation properties can be measured demonstrate the importance of the selection of the appropriate

2013 JINST 8 P09019

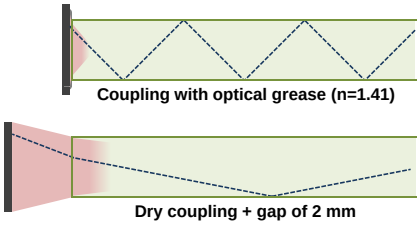

Figure 9. Sketch representing the different paths followed by a typical photon in case of coupling with optical grease (top) and in case of dry coupling (bottom). The collimation effect is especially pronounced if a few millimeter air gap is inserted between the photodetector and the sample.

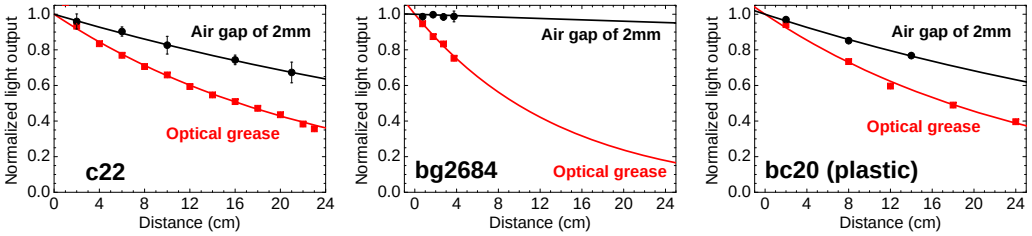

Figure 10. Attenuation profiles of the scintillation light generated by 511 keV γ-photons measured on a LuAG fiber grown by μPD (left), a LuAG crystal grown by Bridgman (middle) and a plastic scintillator (right). Measurements acquired with a photodetector coupling based on silicon grease (n=1.41) are compared with measurements obtained with a 2 mm air gap.

collection angle. The attenuation curve measured with a 2 mm air gap also yielded better results for the LuAG fibers (see left plot of figure 10). The effect is not as pronounced as compared to the behavior of the LuAG crystal grown by Bridgman but attenuation lengths of 53±4 cm could nevertheless be reached. This confirms that the attenuation properties of the fibers can be further improved by a smart choice of light out-coupling method. It is also noteworthy that, as for the case of optical grease coupling, the plastic scintillating fiber measured for reference in the air gap configuration (see right plot of figure 10) did not display a better attenuation length as compared to the LuAG fibers investigated here.

As suggested in section 4.2, the precise selection of the out-coupling technique has to be done carefully since, while a gain in light output might affect the light attenuation, the dry coupling described here yielded a lower amount of photons collected (about the half).

5 Discussion

The attenuation profiles presented in this paper were measured with 511 keV γ-rays. With this excitation method, only a limited number of photoelectrons could be collected by the photodetectors. Methods based on UV, visible light or 10-40 keV X-rays [22] yield significantly higher signals. The drawbacks of these other methods is the relatively short excitation depth and the strong dependence on the surface state. By contrast, the γ-rays selected here excite quasi-homogeneously the 2 mm wide samples since $\lambda_{abs}^{LuAG}(511\,\text{keV}) \sim 1.3$ cm [23]. This situation is more relevant since the LuAG

2013 JINST 8 P09019

fibers were designed to be used in high energetic experiments where the location of the ionization is equally distributed within the scintillator.

Because of the specific experimental conditions, relatively low light yields were measured with the LuAG samples. In order to efficiently distinguish the measured photoelectron yield LY_{pe} from the intrinsic light yield LY_0 of the scintillating material, we tried to summarize the different contributions involved. Similarly to [21], they can be expressed as:

$$LY_{\mathrm{pe}} = \eta_{\mathrm{coll}} \times f_{\mathrm{att}} \times f_{\mathrm{gate}} \times PDE \times LY_0 \tag{5.1}$$

where f_{att} is the fraction of light remaining after propagation, f_{gate} is the fraction of light measured within the considered time window, as compared to the total amount of light emitted (integration on 5μs) and PDE is the photon detection efficiency. The measurement conditions (coupling media and presence of wrapping/coating) then determines the collection efficiency η_{coll} which links the measured light output to the intrinsic light yield LY_0. Estimating each of these factors is important to be able to compare measurements performed on different crystal geometries and different photodetection techniques.

The values of f_{att} were computed from the attenuation lengths of table 2. The values of PDE were computed from the convolution of the emission spectra of the LuAG samples with the photon detection efficiencies from [24] (resp. the quantum efficiency) for the MPPCs (resp. for the PMT). We estimated the scintillation light collection efficiencies η_{coll} for all different readout configuration based on [16, 25, 26].

In table 3, we summarize the estimated values for a set of LuAG fibers grown by μPD and a set of LuAG crystals grown by Bridgman. The two first rows allow comparing the light output measured with a standard PMT (XP2020Q from Photonis) and a MPPC. For both cases, a $2\times2\times8\,\mathrm{mm}^3$ crystal (bg2018) was measured without wrapping and with one of its $2\times2\,\mathrm{mm}^2$ faces in dry contact with the photodetector. We observe that, after correction for the different pulse integration time and the different photon detection efficiency, a similar value of light output can be computed. The rather low light collection efficiency ($\eta_{\mathrm{coll}} \approx 10.6\%$), due to the absence of wrapping and optical grease, then leads to an intrinsic light yield of 29 700 photons per MeV deposit.

In the second part of table 3, we compare the different contributions affecting the light yield for a longer Bridgman-grown LuAG crystal (length of 4.5 cm) and two LuAG fibers grown by μPD. Given the low Cerium doping concentration of the LuAG fibers and based on earlier studies [11], we expect an intrinsic light yield between 13 000 and 15 000 photons per MeV. Such values, could only be obtained with a light collection efficiency of around 15.8%. This contribution is the only free parameter of formula 5.1, f_{att}, f_{gate} and PDE being known. By contrast, we estimate the light collection efficiency of the crystal bg2684 to be around 28%. We explain this difference in η_{coll} by the differences in the samples surface state. This actually confirms that the light collected from the LuAG fibers ends is more collimated. In the LuAG fibers, the scintillation light propagating at large angle is collected with a poorer efficiency, as compared to the LuAG crystals.

We also observe from table 3 that the values of η_{coll} are directly linked to the measured attenuation length. When it is artificially reduced by the presence of a 2 mm air gap between the photodetector and the sample, the loss in η_{coll} is compensated by a gain in λ_{att}. The minimum attenuation length which can be afforded will be fixed by the calorimeter design. Tuning the light collection efficiency will then allow to reach it. For long attenuation lengths, the limitation will

2013 JINST 8 P09019

Table 3. Summary of the different factors explaining the differences in measured light outputs illustrated for two LuAG Bridgman-grown crystals of dimensions $2\times2\times8\,mm^3$ (bg2018) and $2\times2\times45\,mm^3$ (bg2684) and two LuAG fibers grown by μPD of length 22 cm (c20 and c22). The sample c20-h is a 2 cm piece of fiber c20. In the table, the photodetector type is referred as *P* (resp. *M*) for PMT (resp. MPPC). The light was collected from one of the [resp. both] $2\times2\,mm^2$ faces (referred as $1r$ [resp. $2r$]), with glue coupling (referred as *g*), dry contact (referred as *a*) or in presence of a 2 mm air gap (referred as a^+).

Sample ID	Configuration	$\mathbf{LY_{pe}}$ [phe/MeV]	η_{coll}	f_{att}	f_{gate}	PDE	$\mathbf{LY_0}$ [ph/MeV]
bg2018	P 1r a	225	0.106	0.95	0.95	0.078	29 700
bg2018	M 1r a	360	0.106	0.95	0.51	0.232	29 700
bg2684	M 2r g	700	0.28	0.76	0.57	0.232	24 900
c20-h	M 2r g	200	0.158	0.94	0.41	0.232	14 100
c20	M 2r g	115	0.158	0.53	0.41	0.232	14 700
c22	M 2r g	125	0.158	0.63	0.41	0.232	13 100
c22	M 2r a^+	60	0.058	0.81	0.41	0.232	13 100
bg2684	M 2r a^+	70	0.021	1.00	0.57	0.232	24 900

however be the light output. In order to avoid that photon statistics dominate the energy resolution, it is not possible to infinitely decrease η_{coll}.

As in [11], we neglected the effect of self-absorption which was earlier reported for LuAG:Ce in [27]. This is especially valid given the low concentration of Cerium dopant in the LuAG fibers discussed here. We estimated the contribution of self-absorption to the measured light attenuation to be of less than 11 % when the light propagates from the center of the LuAG fibers. This estimation takes into account the change in photon detection efficiency due to the shift in wavelength of the re-absorbed photons. The light attenuation of present fibers is thus mainly explained by the surface defects. Self-absorption has however to be considered as the ultimate limit of the light attenuation.

6 Conclusion and outlook

We presented here the significant improvement of the light propagation in single crystalline LuAG fibers grown by the micro-pulling down technology. Light attenuation lengths in the 20-30 cm range were measured and, by reducing the collection angle, these values could be increased to more than 50 cm. We explain the better propagation of the light by a surface state of higher quality. The difference between the light attenuation length and the light absorption length was earlier explained based on a model where total reflections where assumed not to occur without losses [25]. We attribute these imperfect total reflections to the surface defects. Their size and concentration then determines the probability for the photons to be re-routed by diffraction. Although these defects do not directly absorb the scintillation light, the long travel path induced by elongated geometries

2013 JINST 8 P09019

lead to a poor collection efficiency of this diffracted light. In case of optical grease coupling, the average (in terms of solid angle) number of reflections of the collected light is around 39 for 11 cm of propagation (half length of the LuAG fibers). A measured loss of 37% can then be understood by 39 reflections with 98.8% efficiency each. When an air gap of 2 mm is inserted, the average number of reflection of the collected light is reduced to 18 for the same fiber length. For a fiber of a given surface quality, a better propagation of the light is achieved in the second situation since the light selected interacts less with the surface defects. We also showed here that wrapping and coating are unlikely to improve the light output without degrading the attenuation length. Therefore, in case the calorimeter design requires attenuation lengths even longer than the ones achieved at present, different fiber cladding will be investigated. Although more difficult to process than a naked LuAG fiber, a cladding with a well-matched index of refraction is very likely to further erase the surface defects.

Given the progress made in the material optimization, future work will be more dedicated to the study of possible designs of realistic calorimeters and address the different challenges involved. Compromises will have to be found between the required energy resolution, the length of the fibers, the number of readout channels and the overall cost of the detector . The versatility of the LuAG fibers allow however a variety of different approaches.

Acknowledgments

The research leading to these results was conducted in the scope of the Crystal Clear Collaboration and the International Associated Laboratory IRMAS (CNRS-France & SCS-Armenia). The research has received funding from the French National Agency for Research under grand agreement ANR-10-BLAN-0947 (INFINHI), from Science Committee Armenia under grant agreement 11-1c322 and from the European Union FP7/2007-2013 under grant agreements 256984-EndoTOFPET-US and 295025-IPERA.

References

[1] CALICE collaboration, J. Repond et al., *Design and Electronics Commissioning of the Physics Prototype of a Si-W Electromagnetic Calorimeter for the International Linear Collider*, 2008 *JINST* **3** P08001 [arXiv:0805.4833].

[2] CALICE collaboration, C. Adloff et al., *Construction and Commissioning of the CALICE Analog Hadron Calorimeter Prototype*, 2010 *JINST* **5** P05004 [arXiv:1003.2662].

[3] R. Wigmans, *Sampling calorimetry*, *Nucl. Instrum. Meth.* **A 494** (2002) 277.

[4] R. Wigmans, *The DREAM project: Towards the ultimate in calorimetry*, *Nucl. Instrum. Meth.* **A 617** (2010) 129.

[5] P. Lecoq, *Metamaterials for novel X- or γ-ray detector designs*, *IEEE Nucl. Sci. Confer. R.* (2008) 1405.

[6] P. Lecoq, *New crystal technologies for novel calorimeter concepts*, *J. Phys. Conf. Ser.* **160** (2009) 12016.

[7] M. Nikl et al., *Development of LuAG-based scintillator crystals - a review*, *Prog. Cryst. Growth. Ch.* **59** (2013) 47.

[8] E. Auffray, D. Abler, P. Lecoq, C. Dujardin, J. Fourmigue and D. Perrodin, *Dual readout calorimeter with heavy scintillating crystal fibers*. *IEEE Nucl. Sci. Conf. R. (NSS/MIC)* (2008) 3262.

2013 JINST 8 P09019

[9] M. Letz, A. Gottwald, M. Richter, V. Liberman and L. Parthier, *Temperature-dependent Urbach tail measurements of Lutetium Aluminum garnet single crystals*. *Phys. Rev.* **B 81** (2010) 155109.

[10] Y. Kuwano, K. Suda, N. Ishizawa and T. Yamada, *Crystal growth and properties of* $(Lu,Y)_3Al_5O_{12}$. *J. Cryst. Growth* **260** (2004) 159.

[11] C. Dujardin et al., *LuAG:Ce fibers for high energy calorimetry*, *J. Appl. Phys.* **108** (2010) 13510.

[12] J.A. Mares, et al., *Scintillation properties of* Ce^{3+} *- and* Pr^{3+} *-doped LuAG, YAG and mixed* $Lu_xY_{1-x}AG$ *Garnet Crystals*, *Nuclear Science, IEEE Transactions on* (2012) in press. *IEEE T. Nucl. Sci.* **59** (2012) 2120.

[13] P. Bruza, V. Fidler and M. Nikl, *Table-top instrumentation for time-resolved luminescence spectroscopy of solids excited by nanosecond pulse of soft X-ray source and/or UV laser*, 2011 *JINST* **6** P09007.

[14] W. Drozdowski et al., *Scintillation properties of Praseodymium activated* $Lu_3Al_5O_{12}$ *single crystals*, *IEEE T. Nucl. Sci.* **55** (2008) 2420.

[15] M. Fasoli et al., *Band-gap engineering for removing shallow traps in rare-earth* $Lu_3Al_5O_{12}$ *garnet scintillators using* Ga^{3+} *doping*, *Phys. Rev.* **B 84** (2011) 1.

[16] K. Pauwels, E. Auffray, S. Gundacker, A. Knapitsch and P. Lecoq, *Effect of aspect ratio on the light output of scintillators*, *IEEE T. Nucl. Sci.* **59** (2012) 2340.

[17] R. Simura, A. Yoshikawa and S. Uda, *The radial distribution of dopant (Cr, Nd, Yb, or Ce) in yttrium aluminum garnet* $(Y_3Al_5O_{12})$ *single crystals grown by the micro-pulling-down method*. *J. Cryst. Growth* **311** (2009) 4763. 4769.

[18] D. Maier, D. Rhede, R. Bertram, D. Klimm and R. Fornari, *Dopant segregations in oxide single-crystal fibers grown by the micro-pulling-down method*. *Opt. Mater.* **30** (2007) 11.

[19] X. Xu et al., *Growth parameters optimization for LuAG:Ce scintillating fibers pulled by the micro-pulling down technique* (2013) to be published.

[20] A. Petrosyan, *Crystal growth of laser oxides in the vertical Bridgman configuration*, *J. Cryst. Growth* **139** (1994) 372.

[21] M. Kobayashi, S. Aogaki, F. Takeutchi, Y. Tamagawa and Y. Usuki, *Performance of thin long scintillator strips of GSO:Ce, LGSO:Ce and LuAG:Pr for low energy gamma-rays*, *Nucl. Instrum. Meth.* **A 693** (2012) 226.

[22] P. Anfre et al., *Evaluation of fiber-shaped LYSO for double readout gamma photon detection*, *IEEE T. Nucl. Sci.* **54** (2007) 391.

[23] M.J. Berger et al., *Photon cross sections database*, http://www.nist.gov/pml/data/xcom/index.cfm.

[24] P. Eckert, H.-C. Schultz-Coulon, W. Shen, R. Stamen and A. Tadday, *Characterisation Studies of Silicon Photomultipliers*, *Nucl. Instrum. Meth.* **A 620** (2010) 217 [arXiv:1003.6071].

[25] S. Aogaki, S. Isogai, M. Kobayashi, S. Sugimoto, F. Takeutchi and Y. Tamagawa, *Measurement of 0.511 MeV gamma-rays with a thin long strip of* $Gd_2SiO_5:Ce^{3+}$ *scintillator*, *Nucl. Instrum. Meth.* **A 614** (2010) 250.

[26] A.R. Knapitsch and C. Fabjan, *Photonic Crystals: Enhancing the Light Output of Scintillation Based Detectors*, Ph.D. thesis, Tech. U, Vienna, Austria, CERN-THESIS-2012-279 (2012).

[27] J.A. Mares, et al., *Ce3+-doped scintillators: status and properties of (Y,Lu) aluminium perovskites and garnets*, *Nucl. Instrum. Meth.* **A 537** (2005) 271.

2013 JINST 8 P09019